

# AEGIS: Preserving privacy of 3D Facial Avatars with Adversarial Perturbations

Dawid Wolkiewicz  
Wroclaw University of Science and Technology  
Wroclaw Poland  
dawid.wolkiewicz@pwr.edu.pl

Anastasiya Pechko  
Jagiellonian University  
Krakow Poland  
anastasiya.pechko@doctoral.uj.edu.pl

Piotr Syga  
Wroclaw University of Science and Technology  
Wroclaw Poland  
piotr.syga@pwr.edu.pl

Przemysław Spurek  
Jagiellonian University  
Krakow Poland  
przemyslaw.spurek@uj.edu.pl

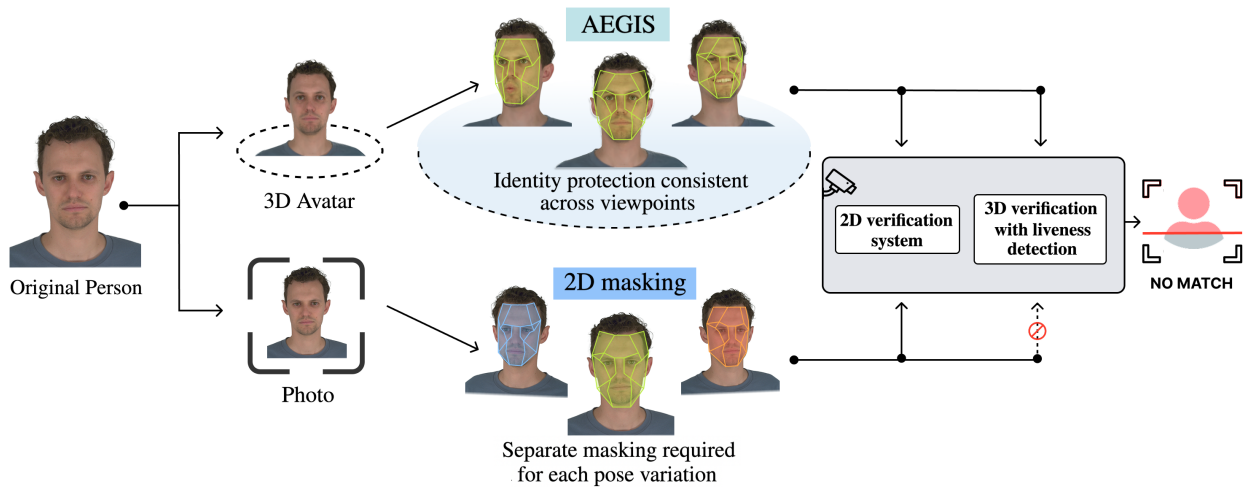


Figure 1. Photos enable 2D face verification but cannot pass 3D verification with liveness detection. Since 3D avatars can be used in such systems, their identity must be protected. Unlike 2D masking, which must be reapplied for each pose, AEGIS achieves consistent identity protection across different viewpoints and poses through geometry-aware 3D masking.

## Abstract

The growing adoption of photorealistic 3D facial avatars, particularly those utilizing efficient 3D Gaussian Splatting representations, introduces new risks of online identity theft, especially in systems that rely on biometric authentication. While effective adversarial masking methods have been developed for 2D images, a significant gap remains in achieving robust, viewpoint-consistent identity protection for dynamic 3D avatars. To address this, we present AEGIS, the first privacy-preserving identity masking framework for 3D Gaussian Avatars that maintains subject’s perceived characteristics. Our method aims to conceal identity-related fa-

cial features while preserving the avatar’s perceptual realism and functional integrity. AEGIS applies adversarial perturbations to the Gaussian color coefficients, guided by a pre-trained face verification network, ensuring consistent protection across multiple viewpoints without retraining or modifying the avatar’s geometry. AEGIS achieves complete de-identification, reducing face retrieval and verification accuracy to 0%, while maintaining high perceptual quality (SSIM = 0.9555, PSNR = 35.52 dB). It also preserves key facial attributes such as age, race, gender, and emotion, demonstrating strong privacy protection with minimal visual distortion.

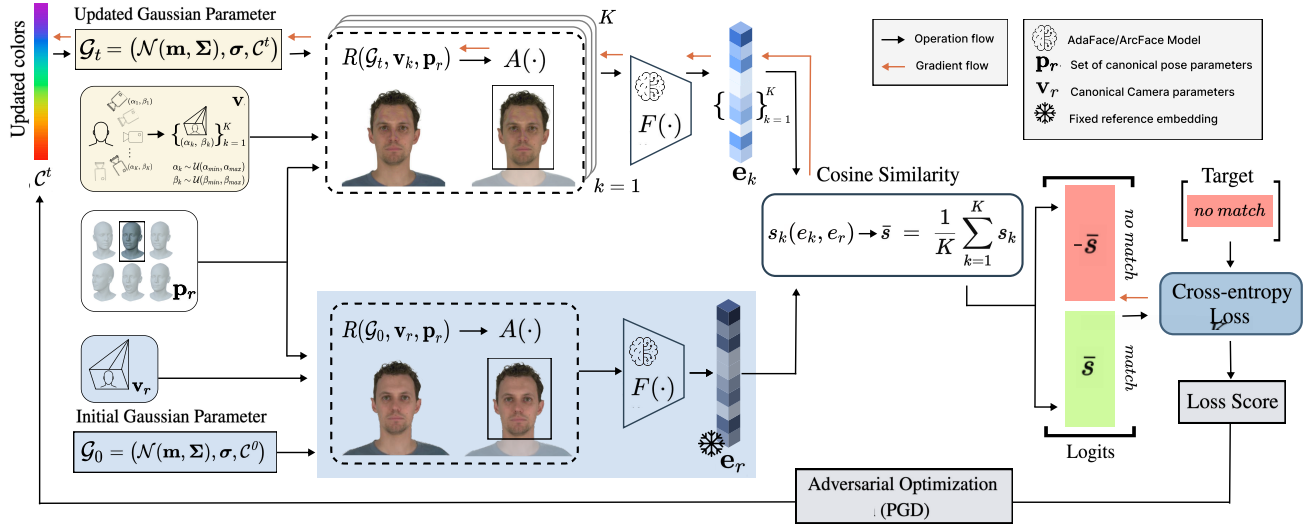


Figure 2. An overview of the AEGIS identity masking pipeline. The process adversarially optimizes the color parameters  $\mathcal{C}^t$  of a 3D Gaussian avatar  $\mathcal{G}$  to evade face recognition by the model  $F(\cdot)$ . A fixed reference embedding  $e_r$  is first obtained by rendering the original avatar  $\mathcal{G}_0$  under canonical camera  $\mathbf{v}_r$  and pose  $\mathbf{p}_r$  parameters, and passing the result through  $F(\cdot)$ . During each PGD optimization step, a set of camera parameters  $\{\mathbf{v}_k\}_{k=1}^K$  is sampled to capture diverse viewpoints. The updated avatar  $\mathcal{G}_t$  is rendered from these viewpoints using the rendering function  $R(\cdot)$  and alignment module  $A(\cdot)$ , producing a batch of images. Identity embeddings  $\{e_k\}$  are then extracted using  $F(\cdot)$ , and their average cosine similarity  $\bar{s}$  with the reference embedding  $e_r$  is computed. This similarity defines the logits ( $\bar{s}$  for "match" and  $-\bar{s}$  for "no match"), from which a cross-entropy loss is computed while targeting the "no match" class. The resulting loss is backpropagated through the network using PGD to update the color parameters  $\mathcal{C}^t$ , yielding an adversarial 3D representation.

## 1. Introduction

In the era of the metaverse [23, 24] and rapid advances in photorealistic visualization, 3D facial avatars are becoming increasingly prevalent in online environments, particularly those built upon the highly efficient 3D Gaussian Splatting (3DGS) [10] representation. The creation and widespread sharing of these visually faithful, controllable digital personas introduce a critical security concern: identity theft through the extraction of biometric information. This threat is particularly severe for systems that rely on face verification and recognition for authentication. While capturing facial data from online videos or calls already presents a privacy risk, the persistent, high-fidelity nature of a controllable 3D avatar constitutes a systemic vulnerability that can be exploited for large-scale spoofing and impersonation.

The challenge of biometric privacy has been studied extensively in the domain of 2D imagery. Existing adversarial masking techniques like Fawkes [20] and LowKey [3], introduce subtle, imperceptible perturbations that shift a user’s features in the embedding space, thereby protecting images from biometric extraction. Other methods employ generative anonymization or adversarial editing to conceal identity-related attributes. However, these 2D pixel-space techniques are unsuitable for 3D avatars because they lack viewpoint consistency, as shown in Fig. 1. Any change in camera angle or avatar animation alters the

2D projection, invalidating the previous perturbations and resulting in unstable protection. Moreover, 2D methods do not modify the underlying 3D representation (the Gaussian primitives) and therefore cannot guarantee persistent or geometry-consistent privacy.

To address this gap, we introduce AEGIS (Adversarial Evasion Gaussian Identity Shield, shown in Fig. 2), the first viewpoint-consistent identity obfuscation method for 3D Gaussian Avatars. Our goal is to conceal identity-related facial information while preserving perceptual realism, resemblance to the original subject and overall usability. AEGIS is a post-training approach that achieves privacy protection by perturbing only the first coefficients of the spherical harmonics representation, which encode the base color of the Gaussian primitives. This ensures that the avatar’s geometry and higher-order view dependence remain unaltered. The obfuscation signal is obtained via constrained Projected Gradient Descent (PGD) [16] optimization against a face verification objective, using ArcFace [4] and AdaFace [11] embeddings. Because this optimization occurs directly in the avatar parameter space and propagates through a differentiable rendering pipeline, the resulting de-identification is viewpoint-consistent, animation-stable, and perceptually coherent.

The source code is available at <https://github.com/Woleek/AEGIS>.

We evaluate AEGIS by measuring retrieval and verification risks using rendered avatars against large-scale 2D face datasets, simulating realistic attack conditions. Our method provides robust privacy guarantees, reducing match rate and rank- $k$  retrieval by up to 100 times, while preserving structural similarity (SSIM) and maintaining attribute-level consistency across age, gender, race, and emotion. This demonstrates that targeted color-space perturbations of 3D Gaussian primitives offer effective privacy from automated recognition systems, without compromising the visual fidelity and utility essential for immersive applications.

Below, we summarize the key contributions of this work:

- **Viewpoint-consistent 3D identity protection.** We propose AEGIS, the first privacy-preserving identity masking framework for 3D Gaussian Avatars, ensuring consistent protection across viewpoints and animations with maintained visual resemblance.
- **Adversarial masking in spherical harmonics space.** AEGIS perturbs only the DC coefficients of spherical harmonics in Gaussian primitives, preserving geometry and view-dependent appearance.
- **Privacy with high perceptual fidelity.** Our optimization guided by ArcFace and AdaFace reduces verification and retrieval accuracy by up to  $100\times$  while maintaining high SSIM and soft-trait consistency.

## 2. Related work

Basic face anonymization methods, such as blurring or black rectangles, are sufficient for static or low-stakes scenarios but offer limited utility in dynamic contexts like social media or video calls and are vulnerable to reversal [21, 29]. Adversarial 2D protection methods, including Fawkes [20] and LowKey [3], reduce recognition by shifting features or applying evasion filters, yet they depend on knowledge of the identification system and cannot ensure viewpoint-consistent anonymization for 3D avatars. Generative anonymization approaches, such as diffusion-based methods [13], G2Face [27], latent code optimization [2], and adversarial makeup editing [22], preserve attributes while changing identity, but operate in 2D and cannot maintain a persistent, controllable avatar or guarantee consistency under head motion. Controllable photorealistic head avatars, like GaussianAvatars [17], enable high-fidelity reenactment across poses and expressions, but prior work has not addressed privacy against biometric verification. Our approach fills this gap by introducing in-renderer adversarial masking on the DC coefficients of spherical harmonics, preserving geometry and view-dependent appearance while enforcing viewpoint-consistent identity suppression without assumptions on the adversary or introducing recovery risks. This provides a practical solution for protecting identity in animated, photorealistic 3D avatars while maintaining visual realism and control.

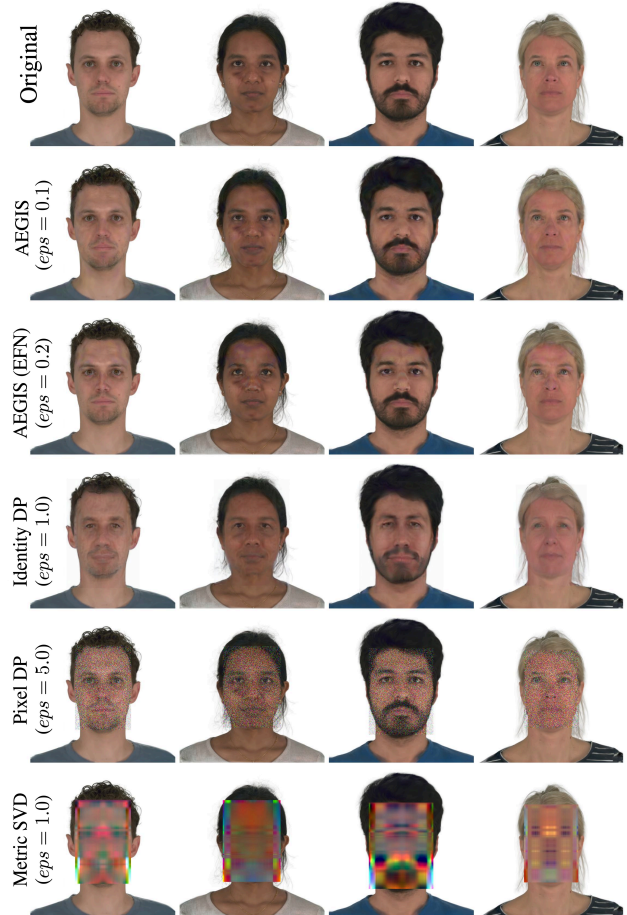


Figure 3. Visualization of example identity masks obtained using AEGIS (for AdaFace) and reference 2D masking methods.

## 3. Method

The proposed avatar identity masking obfuscates identity-related features of a 3D Gaussian-based avatar [17] and preserves perceptual realism. It formulates masking as an adversarial optimization applied to the DC coefficients (the zeroth-order spherical harmonics), that encode the base, view-independent color of each 3D Gaussian primitive [10].

Our pipeline integrates three key components: (1) a differentiable renderer for Gaussian Avatars, (2) a pre-trained face verification network (ArcFace [4] or AdaFace [11]) with built-in face alignment preprocessing, and (3) an adversarial optimization framework. An overview of the proposed method is presented in Fig. 2, which illustrates the loop between rendering, face verification, and adversarial optimization over Gaussian color coefficients.

The core hypothesis is that by perturbing the Gaussian color coefficients in a structured manner, one can generate a mask that renders the avatar unrecognizable to a face verification system, while maintaining visual fidelity. This design employs a privacy-preserving formulation, aiming to

protect the digital avatar’s identity from automated recognition systems. As the reference identity to be obfuscated, we use a frontal render of the original avatar, representing the subject prior to masking. This setting assumes access to the verification network architecture but not to any real enrollment data.

### 3.1. Underlying Models

In our setting, the 3D avatar is represented using the **Gaussian Avatars** framework [17], which combines 3D Gaussian Splatting for scene representation with the FLAME parametric model for facial articulation. Our masking technique is applied to the fully trained avatar and does not affect the initial creation process.

**Gaussian Splatting** [10] is a differentiable rendering method for 3D scene reconstruction. The scene consists of  $(n)$  anisotropic 3D Gaussian primitives, each defined by a mean position  $(m_i)$ , covariance matrix  $(\Sigma_i \in \mathbb{R}^{3 \times 3})$ , opacity  $(\sigma_i \in \mathbb{R})$ , and diffuse color coefficients  $C_i \in \mathbb{R}^k$ , where  $k$  denotes the number of spherical harmonics (SH) coefficients representing view-dependent color. The complete representation can be formally expressed as the following set of triples:

$$\mathcal{G} = \{(\mathcal{N}(m_i, \Sigma_i), \sigma_i, C_i)\}_{i=1}^n,$$

The covariance matrix is defined as  $\Sigma_i = R_i S_i S_i^\top R_i^\top$ , where  $R_i, S_i \in \mathbb{R}^{3 \times 3}$ , ensuring positive definiteness. During rendering, each 3D Gaussian is projected onto the 2D image plane by transforming its covariance into screen space:  $\Sigma'_i = J W_i \Sigma_i W_i^\top J^\top$ , where  $\Sigma_i \in \mathbb{R}^{3 \times 3}$ ,  $W_i \in \mathbb{R}^{3 \times 3}$  is the world-to-camera transform, and  $J \in \mathbb{R}^{2 \times 3}$  is the Jacobian of the perspective projection, resulting in the screen-space covariance  $\Sigma'_i \in \mathbb{R}^{2 \times 2}$ . The final pixel color  $C_{\text{px}}$  is obtained through differentiable alpha blending of 3D Gaussians, sorted by depth. We assume that these are indexed by  $i \in \{1, \dots, N\}$ :

$$C_{\text{px}} = \sum_{i=1}^N c_i \alpha_i \prod_{j=1}^{i-1} (1 - \alpha_j),$$

where  $c_i$  denotes the color of the  $i$ -th Gaussian, and  $\alpha_i$  is computed by evaluating a 2D Gaussian with covariance  $\Sigma_i$ , scaled by a learned per-Gaussian opacity  $\alpha_i$  [28].

The optimization of 3D Gaussians is guided by minimizing a photometric reconstruction loss to achieve an optimal spatial distribution of Gaussians. Further training and optimization details are provided in [10].

**FLAME** (Faces Learned with an Articulated Model and Expressions) [14] is a 3D morphable head model with  $N = 5,023$  vertices and  $K = 4$  joints. It maps low-dimensional shape  $(\beta \in \mathbb{R}^{|\beta|})$ , pose  $(\mathbf{p} \in \mathbb{R}^{|\mathbf{p}|})$ , and expression  $(\psi \in \mathbb{R}^{|\psi|})$  parameters to a full 3D mesh using Linear Blend

Skinning (LBS) with corrective blendshapes. Formally, it is defined as a function  $M(\beta, \mathbf{p}, \psi) : \mathbb{R}^{|\beta| \times |\mathbf{p}| \times |\psi|} \rightarrow \mathbb{R}^{3N}$ :

$$M(\beta, \mathbf{p}, \psi) = W(T_P(\beta, \mathbf{p}, \psi), J(\beta), \mathbf{p}, \mathcal{W}),$$

where  $T_P$  denotes the posed template obtained by adding shape-, pose-, and expression-dependent offsets to the base mesh  $\bar{\mathbf{T}} \in \mathbb{R}^{3N}$ .  $W(\cdot)$  is the standard skinning function that rotates the vertices of  $T_P$  around joints  $J \in \mathbb{R}^{3K}$  and applies linear smoothing using blend weights  $\mathcal{W} \in \mathbb{R}^{K \times N}$ .

In our work, the avatar is created from multi-view video data. The FLAME model provides semantic correspondence, enabling the identification of Gaussian primitives corresponding to specific facial regions (e.g., eyes, lips). The DC coefficients of the selected Gaussians are assembled into a tensor  $\mathcal{C} \in \mathbb{R}^{N \times 3}$  which serves as the optimization variable during the adversarial masking process.

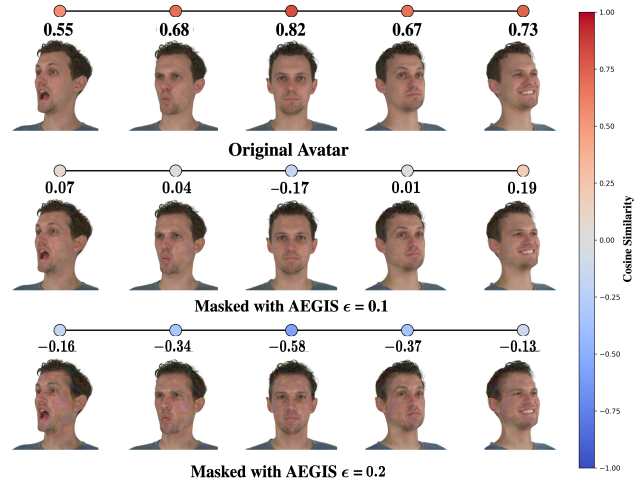


Figure 4. Effect of pose variation and privacy budget  $\epsilon$  on identity masking persistence (against AdaFace verification system). Top: unmasked avatar with high similarity during verification across poses. Middle: masked avatar with  $\epsilon = 0.1$  shows reduced similarity but residual identity cues at some angles. Bottom: with  $\epsilon = 0.2$ , avatar is completely de-identified across all poses. These results demonstrate the trade-off between visual fidelity and privacy strength, as higher  $\epsilon$  values yield stronger privacy at the cost of greater perceptual deviation.

### 3.2. Facial Verification

To quantitatively measure identity, the avatar is rendered from a specific viewpoint with a consistent pose, and its identity embedding is extracted. Let  $R(\mathcal{G}, \mathbf{v}, \mathbf{p})$  be the differentiable rendering process, which synthesizes a 2D image  $\mathcal{I}$  of the avatar. This rendering is a function of: (1) the 3D Gaussian model  $\mathcal{G}$ , (2) a set of camera parameters  $\mathbf{v}$  defining the viewpoint and projection, and (3) a set of pose parameters  $\mathbf{p}$  controlling the underlying FLAME model.

Our optimization variable is the DC coefficients tensor  $\mathcal{C}$ , which defines the view-independent base color of the Gaussian primitives. We can therefore denote the parametrized model as  $\mathcal{G}_{\mathcal{C}}$ .

To process the rendered image  $\mathcal{I}$ , we apply a face alignment function  $A(\cdot)$  that produces face crops of size  $112 \times 112$  pixels, after pose normalization. The alignment is based on five facial landmarks predicted by the RetinaFace model [5], as in [4, 11]. This operation compensates for variations in scale and in-plane rotation, yielding a canonical input for the verification network. Subsequently, the aligned image  $A(\mathcal{I})$  is then passed to a pre-trained face verification network  $F(\cdot)$  (e.g., ArcFace or AdaFace), which produces a high-dimensional feature vector  $\mathbf{e} \in \mathbb{R}^{512}$ . The identity embedding is obtained as  $\mathbf{e} = F(A(\mathcal{I}))$ . These networks were selected for their robustness and established ability to map facial images into an embedding space where cosine similarity reflects identity proximity.

For the adversarial optimization, we employ Expectation Over Transformation (EOT) [1], to ensure that the generated mask remains robust under different viewpoints. We define a transformation distribution  $\mathbf{T}$  over viewpoints  $\mathbf{v}$ , corresponding to camera parameters, for which we uniformly sample an angle  $\alpha$  for x-rotation (pitch) and an angle  $\beta$  for y-rotation (yaw), both within the range  $[-0.5, 0.5]$  radians. At each optimization step, we draw  $K = 5$  viewpoints  $\mathbf{v}_1, \dots, \mathbf{v}_K \sim \mathbf{T}$ . A neutral reference pose  $\mathbf{p}_r$  is used. The identity embedding for a given viewpoint  $\mathbf{v}$  is computed as a differentiable function of the color tensor  $\mathcal{C}$ :

$$\mathbf{e}_a(\mathcal{C}, \mathbf{v}) = F(A(R(\mathcal{G}_{\mathcal{C}}, \mathbf{v}, \mathbf{p}_r))), \quad (1)$$

and the feature vector  $\mathbf{e}_a$  is L2-normalized after extraction to produce the unit-length identity embedding.

The reference identity embedding  $\mathbf{e}_r$  is computed once from the original, unmasked avatar (with the original colors  $\mathcal{C}^0$ ) and rendered with identical pose and default frontal viewpoint.  $\mathbf{e}_r$  vector serves as the constant target to which the masked avatar’s embedding is compared. The cosine similarity between the embeddings quantifies the identity similarity:

$$s(\mathbf{e}_a(\mathcal{C}, \mathbf{v}), \mathbf{e}_r) = \frac{\mathbf{e}_a(\mathcal{C}, \mathbf{v}) \cdot \mathbf{e}_r}{\|\mathbf{e}_a(\mathcal{C}, \mathbf{v})\| \|\mathbf{e}_r\|}, \quad (2)$$

where  $\cdot$  is the scalar product.

### 3.3. Adversarial Masking

To conceal the avatar’s identity, we perform adversarial optimization on the DC coefficients tensor  $\mathcal{C}$ . The objective is to find an optimal perturbed color tensor  $\mathcal{C}^*$  that minimizes the expected identity similarity over the transformation distribution  $\mathbf{T}$ , thereby pushing the avatar’s embedding  $\mathbf{e}_a$  away from the reference embedding  $\mathbf{e}_r$ . This constrained

optimization problem is formulated as:

$$\begin{aligned} \mathcal{C}^* &= \arg \min_{\mathcal{C}} \mathbf{E}_{\mathbf{v} \sim \mathbf{T}} [s(\mathbf{e}_a(\mathcal{C}, \mathbf{v}), \mathbf{e}_r)] \\ \text{s.t. } &\|\mathcal{C} - \mathcal{C}^0\|_{\infty} \leq \epsilon. \end{aligned} \quad (3)$$

The constraint employs the  $\ell_{\infty}$  (supremum) norm, which measures the maximum absolute element-wise difference between two tensors. It restricts the optimization to a bounded neighborhood (hypercube) around the original color tensor, preventing the optimizer from introducing drastic local color shifts or structural artifacts. For a tensor  $\mathcal{X}$  with components  $x_i$ , this norm is defined as  $\|\mathcal{X}\|_{\infty} = \max_i |x_i|$ . Accordingly,  $\|\mathcal{C} - \mathcal{C}^0\|_{\infty}$  computes the maximum absolute change across all color channels and Gaussian components. The hyperparameter  $\epsilon$  defines the perturbation budget, i.e., the maximum allowed per-channel deviation, bounded by the dynamic range of the original tensor:  $0 \leq \epsilon \leq \max(\mathcal{C}^0) - \min(\mathcal{C}^0)$ , ensuring all perturbed colors remain valid. Its value is selected empirically to balance privacy preservation and visual realism.

We solve this optimization problem using the PGD [16]. To guide the optimization, we define the objective as cross-entropy loss  $\mathcal{L}$  based on the cosine similarity  $s = s(\mathbf{e}_a(\mathcal{C}, \mathbf{v}), \mathbf{e}_r)$  between embeddings. For a single viewpoint  $\mathbf{v}$ , the loss is:

$$\mathcal{L}(\mathcal{C}, \mathbf{v}) = \log(1 + e^{-2s\lambda}), \quad (4)$$

with logits  $[-s\lambda, s\lambda]$  and a scaling constant  $\lambda = 10$ . The expected loss under the transformation distribution is:

$$\mathcal{L}_{EOT}(\mathcal{C}) = \mathbf{E}_{\mathbf{v} \sim \mathbf{T}} [\mathcal{L}(\mathcal{C}, \mathbf{v})]. \quad (5)$$

Maximizing this loss is equivalent to minimizing the identity similarity. The gradient  $\nabla_{\mathcal{C}} \mathcal{L}_{EOT}$  thus provides the direction in color space that most effectively increases dissimilarity from the reference identity.

At each iteration  $t$ , PGD performs (1) a gradient ascent step to maximize the loss, followed by (2) a projection step enforcing the  $\ell_{\infty}$  constraint. The gradient is estimated stochastically over  $K$  sampled viewpoints:

$$\nabla_{\mathcal{C}} \mathcal{L}_{EOT}(\mathcal{C}^{(t)}) \approx \frac{1}{K} \sum_{i=1}^K \nabla_{\mathcal{C}} \mathcal{L}(\mathcal{C}^{(t)}, \mathbf{v}_i), \quad (6)$$

and the update rule is:

$$\mathcal{C}^{(t+1)} = \phi_{\mathcal{C}^0, \epsilon} \left( \mathcal{C}^{(t)} + \alpha \cdot \text{sign}(\nabla_{\mathcal{C}} \mathcal{L}_{EOT}(\mathcal{C}^{(t)})) \right), \quad (7)$$

where  $\alpha$  is the step size controlling the update magnitude, set relative to the perturbation budget as  $\alpha = (0.01/0.3)\epsilon$ . The sign function specifies the optimal step direction within the  $\ell_{\infty}$ -norm ball. The projection operator  $\phi_{\mathcal{C}^0, \epsilon}(\cdot)$  enforces the constraint by clipping each element:

$$\phi_{\mathcal{C}^0, \epsilon}(\cdot) = \text{clip}(\cdot, \mathcal{C}^0 - \epsilon, \mathcal{C}^0 + \epsilon), \quad (8)$$

where  $\text{clip}(x, a, b)$  denotes an element-wise operation that restricts each entry  $x_i$  to the range  $[a_i, b_i]$ , i.e.,  $\text{clip}(x_i, a_i, b_i) = \min(\max(x_i, a_i), b_i)$ . This ensures that each updated tensor  $\mathcal{C}^{(t+1)}$  remains within the  $\epsilon$ -ball centered at  $\mathcal{C}^0$ , satisfying the constraint at every iteration.

After  $T_{\max}$  iterations, the final optimized tensor  $\mathcal{C}^* = \mathcal{C}^{(T_{\max})}$  replaces the original DC coefficients in the avatar model, yielding a de-identified avatar representation that persistently conceals identity.

## 4. Evaluation

To systematically assess the proposed avatar identity masking framework, we evaluate the masked avatars from three complementary perspectives: (1) identity retrieval, (2) face verification, and (3) visual utility preservation.

Our evaluation methodology takes inspiration from [26], where the authors proposed testing anonymization methods across the dual axes of privacy protection and utility preservation. We extend this approach to improve the reliability and comparability of results between 2D and 3D settings. Unlike [26], where 2D methods were tested on large-scale benchmarks and 3D methods on a small, self-collected dataset, we unify the evaluation by combining rendered avatar datasets with established 2D face databases.

In the privacy-preserving evaluations, existing large-scale 2D face datasets are employed to emulate a real-world verification system with multiple enrolled identities. Specifically, we use CelebA [15], a large-scale dataset of over 200k celebrity faces serving as a diverse retrieval gallery, and LFW (Labeled Faces in the Wild) [9], a benchmark dataset of unconstrained face photographs for threshold calibration and verification testing.

Additionally, we construct a reference dataset of 10 individuals whose photos, obtained from the NeRSemble dataset [12], were used to train Gaussian Avatars. This dataset provides frames from 11 different motion-capture recordings, each capturing displays of distinct emotions and expressions.

To ensure compatibility with facial verification models, we retain only near-frontal images. Yaw, pitch, and roll thresholds for frontal views are determined by rendering the corresponding avatars with default camera parameters and estimating pose from RetinaFace facial landmarks. These thresholds are then slightly relaxed according to the observed deviation in real images. For each subject, we sample 22 frames (2 per expression category) to approximate the mean number of images per identity in CelebA (19.91). We refer to this curated dataset as NeRSembleGT. In all experiments, the effectiveness of identity masking is assessed using 2D renderings of avatars, as all metrics and face verification models require 2D image inputs.

### 4.1. Identity Retrieval

The rank- $k$  evaluation measures how easily anonymized avatars can be linked back to their original identity among a gallery of images. This experiment reflects a realistic retrieval scenario in which a privacy-preserving system must ensure that anonymized faces are sufficiently displaced in the embedding space, preventing re-identification.

For each anonymized render (query), we extract a face embedding  $\mathbf{e}_q$  using the same face recognition model employed during masking, or the alternative one to evaluate transferability across recognition systems. A gallery of real embeddings  $\{\mathbf{e}_g\}$  is constructed from the CelebA test split and NeRSembleGT datasets. Cosine distance is used to rank all gallery embeddings by similarity to query:

$$d_i = 1 - \frac{\mathbf{e}_q \cdot \mathbf{e}_{g_i}}{\|\mathbf{e}_q\| \|\mathbf{e}_{g_i}\|}. \quad (9)$$

The retrieval rank of the correct identity defines the identification score.

We report the *Accuracy@k* metric for  $k \in [1, 50]$ :

$$\text{Accuracy@}k = \frac{1}{N} \sum_{i=1}^N \mathbf{I}[\text{rank}(i) \leq k], \quad (10)$$

where  $N$  denotes the total number of anonymized queries and  $\mathbf{I}$  is the indicator function. Lower rank- $k$  accuracy indicates stronger de-identification, as the masked avatars are less likely to be linked to their original identity. A larger value of  $k$  (e.g.,  $k = 50$ ) corresponds to a more lenient retrieval criterion and thus represents a more challenging evaluation setting for the masking method.

### 4.2. Face Verification

While rank- $k$  retrieval evaluates resistance to identification, face verification assesses whether the anonymized avatar can still be accepted as the same individual under standard biometric protocols.

The decision threshold  $\tau$  for cosine similarity is calibrated using the LFW dataset. Positive and negative embedding pairs are sampled, and the Equal Error Rate (EER) point is computed by fitting the False Accept Rate (FAR) and False Reject Rate (FRR) curves:

$$\text{FAR}(\tau) = \frac{\# \text{ False Accepts}}{\# \text{ Negatives}}, \quad \text{FRR}(\tau) = \frac{\# \text{ False Rejects}}{\# \text{ Positives}}. \quad (11)$$

The threshold  $\tau_{EER}$  corresponds to the intersection point where  $\text{FAR} = \text{FRR}$ , representing an optimal balance between false matches and false rejections. This value is then used for all subsequent verification tests.

Next, we evaluate the masked avatars against their original references from NeRSembleGT using this fixed verification threshold. For each pair  $(\mathbf{e}_a, \mathbf{e}_r)$ , the cosine similarity  $s(\mathbf{e}_a, \mathbf{e}_r)$  is computed. An avatar is classified as

Method	Rank 1 (%) ↓	Rank 50 (%) ↓	Match rate (%) ↓	SSIM ↑	PSNR (dB) ↑	Age (diff.) ↓	Race (%) ↑	Gender (%) ↑	Emotion (%) ↑
Real images	100	100	100	–	–	–	–	–	–
Avatar renders	100	100	100	1	∞	0	100	100	100
AEGIS $\epsilon = 0.05$	100	100	100	0.9870	41.24	0.70	70	100	100
AEGIS $\epsilon = 0.1$	40	70	70	0.9590	35.67	2.68	60	90	100
<b>AEGIS <math>\epsilon = 0.2</math></b>	<b>0</b>	<b>0</b>	<b>0</b>	<b>0.8881</b>	<b>30.58</b>	<b>5.41</b>	<b>40</b>	<b>100</b>	<b>90</b>
AEGIS $\epsilon = 0.3$	0	0	0	0.8247	28.06	6.66	30	90	90
AEGIS (EFN) $\epsilon = 0.2$	80	100	90	0.9587	35.48	2.67	60	90	80
AEGIS (FLN) $\epsilon = 0.3$	70	100	100	0.9341	33.01	2.49	60	90	90
IdentityDP $\epsilon = 100$	0	50	40	0.8224	27.76	3.00	40	90	70
IdentityDP $\epsilon = 1$	0	20	10	0.8138	27.37	2.30	20	90	60
PixelDP (weak, $\epsilon = 20$ )	100	100	100	0.2807	23.13	2.70	90	100	90
PixelDP (strong, $\epsilon = 5$ )	100	100	100	0.0459	12.72	6.50	70	90	50
MetricSVD (weak, $\epsilon = 20$ )	90	100	100	0.8196	26.57	3.70	50	90	50
MetricSVD (strong, $\epsilon = 1$ )	0	10	10	0.6257	16.35	11.80	40	80	20

Table 1. Masking results on the ArcFace verification system. Arrows ( $\uparrow, \downarrow$ ) indicate desirable metric directions, and **bold** highlights the best-performing configuration. For the AEGIS method, letters denote perturbation regions (E: eyes, F: forehead, N: nose, L: lips); if unspecified, the method was applied to all Gaussians.

Method	Rank 1 (%) ↓	Rank 50 (%) ↓	Match rate (%) ↓	SSIM ↑	PSNR (dB) ↑	Age (diff.) ↓	Race (%) ↑	Gender (%) ↑	Emotion (%) ↑
Real images	100	100	100	–	–	–	–	–	–
Avatar renders	100	100	100	1	∞	0	100	100	100
AEGIS $\epsilon = 0.05$	100	100	100	0.9859	41.38	1.33	100	80	100
<b>AEGIS <math>\epsilon = 0.1</math></b>	<b>0</b>	<b>0</b>	<b>0</b>	<b>0.9555</b>	<b>35.52</b>	<b>2.62</b>	<b>60</b>	<b>100</b>	<b>80</b>
AEGIS $\epsilon = 0.2$	0	0	0	0.8812	30.08	3.71	50	100	80
AEGIS $\epsilon = 0.3$	0	0	0	0.8139	27.29	4.64	40	100	80
AEGIS (EFN) $\epsilon = 0.2$	0	10	10	0.9563	35.25	2.04	70	100	90
AEGIS (FLN) $\epsilon = 0.3$	0	0	0	0.9287	32.61	1.97	50	90	80
IdentityDP $\epsilon = 100$	10	40	40	0.8224	27.76	3.00	40	90	70
IdentityDP $\epsilon = 1$	0	10	0	0.8138	27.37	2.30	20	90	60
PixelDP (weak, $\epsilon = 20$ )	100	100	100	0.2807	23.13	2.70	90	100	90
PixelDP (strong, $\epsilon = 5$ )	70	90	90	0.0459	12.72	6.50	70	90	50
MetricSVD (weak, $\epsilon = 20$ )	80	100	100	0.8196	26.57	3.70	50	90	50
MetricSVD (strong, $\epsilon = 1$ )	10	30	30	0.6257	16.35	11.80	40	80	20

Table 2. Masking results on the AdaFace verification system. Arrows ( $\uparrow, \downarrow$ ) indicate desirable metric directions, and **bold** highlights the best-performing configuration. For the AEGIS method, letters denote perturbation regions (E: eyes, F: forehead, N: nose, L: lips); if unspecified, the method was applied to all Gaussians.

a *match* achieves a similarity score  $s \geq \tau_{EER}$  with any of real reference images belonging to the same identity, and as a *no-match* otherwise. The final verification accuracy quantifies the proportion of anonymized avatars still recognized as their originals. Lower verification accuracy indicates stronger privacy protection and reduced biometric traceability.

### 4.3. Utility Preservation

Identity masking should protect privacy while preserving visual quality and perceptual usability. We therefore assess the utility preservation of the anonymized avatars relative to their unaltered counterparts using both low-level fidelity and high-level semantic consistency metrics.

For each pair of original and anonymized renders, two traditional image quality metrics are calculated: (1) Struc-

Masked on	ArcFace ( $\epsilon = 0.05$ )	ArcFace ( $\epsilon = 0.1$ )	ArcFace ( $\epsilon = 0.2$ )	ArcFace ( $\epsilon = 0.3$ )	AdaFace ( $\epsilon = 0.05$ )	AdaFace ( $\epsilon = 0.1$ )	AdaFace ( $\epsilon = 0.2$ )	AdaFace ( $\epsilon = 0.3$ )
Evaluated on	AdaFace				ArcFace			
Rank 1 (%) ↓	100	0	0	0	100	60	0	0
Rank 50 (%) ↓	100	10	0	0	100	80	0	0
Match rate (%) ↓	100	0	0	0	100	80	0	0

Table 3. Cross-system evaluation, where the masking is optimized against one face verification system and tested against another.

tural Similarity Index (SSIM) that measures perceptual structural consistency, and (2) Peak Signal-to-Noise Ratio (PSNR), quantifying pixel-level fidelity.

Before metric computation, both images are aligned and cropped to bounding box obtained from RetinaFace detector. Reported SSIM and PSNR values are averaged across all paired samples.

To evaluate soft-trait preservation, we use the DeepFace framework [19] to predict facial attributes from original and anonymized render pairs. We compute four metrics: the emotion match rate (agreement in predicted dominant emotion), gender match rate (agreement in predicted gender), race match rate (agreement in predicted racial category), and age difference (the absolute difference between predicted ages).

High SSIM/PSNR and semantic consistency indicate that the masking procedure preserves visual realism and usability, while low identification and verification scores confirm effective identity protection.

## 5. Experiments

We evaluate AEGIS under varying privacy budgets, recognition systems, and masking configurations. Experiments are conducted on ten avatars generated using the Gaussian Avatars method, each for a unique identity. Fig. 3 shows example avatar renderings, presenting qualitative results that compare AEGIS with 2D masking baselines.

We apply AEGIS masking with privacy budgets  $\epsilon \in \{0.05, 0.1, 0.2, 0.3\}$ . For each  $\epsilon$ , we perform 300 steps of adversarial optimization against two state-of-the-art face recognition models, ArcFace [4] and AdaFace [11], treated as independent adversaries, following the procedure described in Sec. 3. The method is benchmarked against IdentityDP [25], PixelDP [6], and MetricSVD [7]. Evaluation follows the protocol from Sec. 4, assessing identity retrieval (Rank-1, Rank-50), face verification (Match rate), and visual utility metrics (SSIM, PSNR, attribute consistency).

Table 1 summarizes the results when ArcFace serves as the adversarial recognizer. At  $\epsilon = 0.1$ , Rank-1 retrieval decreases to 40% while maintaining high structural similarity (SSIM 0.9590). Increasing the privacy budget to  $\epsilon = 0.2$  reduces Rank-1, Rank-50 and Match rate to 0%. Compared with the baselines, IdentityDP and MetricSVD

exhibit greater degradation in image quality for comparable privacy levels, while PixelDP fails to suppress identity signal (100% Rank-1) and severely reduces image fidelity (SSIM 0.0459).

Table 2 reports the corresponding results when targeting AdaFace. AEGIS achieves full de-identification (0% Rank-1, 0% Rank-50, 0% Match rate) at  $\epsilon = 0.1$ , while preserving high visual quality (SSIM 0.9555, PSNR 35.52 dB) and semantic consistency. None of the baseline methods reach a comparable trade-off between privacy and perceptual fidelity under equivalent privacy constraints.

To assess transferability, we conduct cross-system evaluations (Table 3). Masks optimized for the ArcFace adversary exhibit strong generalization to AdaFace. For instance, at  $\epsilon = 0.1$ , the ArcFace-trained masks reduce AdaFace’s Rank-1 accuracy to 0% without additional optimization. In contrast, masks trained against AdaFace transfer less effectively to ArcFace, requiring larger perturbations to achieve comparable de-identification performance. This asymmetry may stem from differences in the models’ margin formulations. ArcFace applies a uniform additive angular margin [4], while AdaFace adjusts this margin adaptively according to sample difficulty, based on feature norms [11].

**Ablation Study** We perform ablation studies to examine two key aspects of AEGIS: (1) the impact of applying masks to targeted facial regions, and (2) the stability of the identity masking under pose variations.

We analyze the contribution of different facial regions by perturbing selected subsets of the avatar’s Gaussians, identified by FLAME binding (e.g., eyes, forehead, nose). Representative combinations are reported in Tables 1 and 2. Results indicate that region-specific masking is feasible but less efficient than full-avatar masking. To achieve comparable de-identification, targeted masking requires substantially larger privacy budgets ( $\epsilon = 0.3$  or higher) than full-avatar masking ( $\epsilon = 0.1$ ). These findings suggest that identity-relevant information is distributed across the full avatar representation, and masking the entire model provides a more efficient privacy-utility balance.

We further evaluate the consistency of the learned masks across pose changes (Fig. 4). For the unmasked avatar, cosine similarity between embeddings remains high across

poses (0.55–0.82), indicating stable identity. Applying AEGIS with a low budget ( $\epsilon = 0.1$ ) substantially reduces similarity (e.g., from 0.82 to  $-0.17$  in the frontal view). However, at certain angles, similarity (e.g., 0.19) may remain above typical verification thresholds, suggesting partial identity leakage. A higher privacy budget ( $\epsilon = 0.2$ ) produces a more consistent de-identification effect, with negative values of cosine similarity across all poses and viewpoints ( $-0.58$  to  $-0.13$ ). These results highlight the trade-off: lower  $\epsilon$  values preserve appearance with minimal visible change but may leave residual identity cues at extreme poses, while higher  $\epsilon$  values ensure stronger privacy at the cost of increased perceptual deviation. In practice, such deviations may resemble natural degradations (e.g., compression artifacts in video communication) and remain visually acceptable for typical downstream applications.

For additional experiments, visualized examples and extended ablation study see [Appendix A](#) and [Appendix B](#).

## 6. Conclusion

We introduced AEGIS, an identity masking method for 3D Gaussian Avatars that perturbs only the base color coefficients through PGD, while preserving geometry, view-dependent appearance, and the perceived identity of the avatar. This approach allows users to present realistic 3D avatars in applications such as video calls, social VR, or other interactive environments, while safeguarding against automatic verification and identity theft. By optimizing the avatar representation directly, AEGIS ensures viewpoint consistency and animation stability by design. Experimental results indicate that the proposed method effectively reduces automatic recognition accuracy while preserving perceptual fidelity and high-level semantic features. These findings confirm that geometry-consistent adversarial color perturbations offer a practical and visually coherent approach to protect the privacy of photorealistic 3D facial avatars without diminishing their realism or functional utility.

**Limitations and Future Work** AEGIS perturbs only the DC coefficients of spherical harmonics, preserving geometry but restricting the masking signal and leaving minor residual identity cues at extreme poses. Cross-system transfer remains asymmetric, motivating future validation across diverse avatar systems and 3D verification settings to improve transferability and robustness.

## References

- [1] Anish Athalye, Logan Engstrom, Andrew Ilyas, and Kevin Kwok. Synthesizing robust adversarial examples. In *International conference on machine learning*, pages 284–293. PMLR, 2018. 5
- [2] Simone Barattin, Christos Tzelepis, Ioannis Patras, and Nicu Sebe. Attribute-preserving face dataset anonymization via latent code optimization. In *Proceedings of the IEEE/CVF Conference on Computer Vision and Pattern Recognition (CVPR)*, pages 8001–8010, 2023. 3
- [3] Valeriia Cherepanova, Micah Goldblum, Harrison Foley, Shiyuan Duan, John P Dickerson, Gavin Taylor, and Tom Goldstein. Lowkey: Leveraging adversarial attacks to protect social media users from facial recognition. *Proceedings of the International Conference on Learning Representations (ICLR)*. 2, 3
- [4] Jiankang Deng, Jia Guo, Niannan Xue, and Stefanos Zafeiriou. Arcface: Additive angular margin loss for deep face recognition. In *Proceedings of the IEEE/CVF conference on computer vision and pattern recognition*, pages 4690–4699, 2019. 2, 3, 5, 8
- [5] Jiankang Deng, Jia Guo, Evangelos Ververas, Irene Kotsia, and Stefanos Zafeiriou. Retinaface: Single-shot multi-level face localisation in the wild. In *Proceedings of the IEEE/CVF conference on computer vision and pattern recognition*, pages 5203–5212, 2020. 5
- [6] Liyue Fan. Image pixelization with differential privacy. In *IFIP Annual Conference on Data and Applications Security and Privacy*, pages 148–162. Springer, 2018. 8
- [7] Liyue Fan. Practical image obfuscation with provable privacy. In *2019 IEEE international conference on multimedia and expo (ICME)*, pages 784–789. IEEE, 2019. 8
- [8] Ian J. Goodfellow, Jonathon Shlens, and Christian Szegedy. Explaining and harnessing adversarial examples. In *3rd International Conference on Learning Representations, ICLR, Conference Track Proceedings*, 2015. 11
- [9] Gary B Huang, Marwan Mattar, Tamara Berg, and Eric Learned-Miller. Labeled faces in the wild: A database for studying face recognition in unconstrained environments. In *Workshop on faces in 'Real-Life' Images: detection, alignment, and recognition*, 2008. 6
- [10] Bernhard Kerbl, Georgios Kopanas, Thomas Leimkühler, and George Drettakis. 3d gaussian splatting for real-time radiance field rendering. *ACM Transactions on Graphics*, 42(4), 2023. 2, 3, 4
- [11] Minchul Kim, Anil K Jain, and Xiaoming Liu. Adaface: Quality adaptive margin for face recognition. In *Proceedings of the IEEE/CVF conference on computer vision and pattern recognition*, pages 18750–18759, 2022. 2, 3, 5, 8
- [12] Tobias Kirschstein, Shenhan Qian, Simon Giebenhain, Tim Walter, and Matthias Nießner. Nersemble: Multi-view radiance field reconstruction of human heads. *ACM Trans. Graph.*, 42(4), 2023. 6
- [13] Han-Wei Kung, Tuomas Varanka, Sanjay Saha, Terence Sim, and Nicu Sebe. Face anonymization made simple. In *2025 IEEE/CVF Winter Conference on Applications of Computer Vision (WACV)*, pages 1040–1050, 2025. 3
- [14] Tianye Li, Timo Bolkart, Michael J. Black, Hao Li, and Javier Romero. Learning a model of facial shape and expression from 4D scans. *ACM Transactions on Graphics, (Proc. SIGGRAPH Asia)*, 36(6):194:1–194:17, 2017. 4
- [15] Ziwei Liu, Ping Luo, Xiaogang Wang, and Xiaoou Tang. Deep learning face attributes in the wild. In *Proceedings of*

- International Conference on Computer Vision (ICCV)*, 2015. 6
- [16] Aleksander Madry, Aleksandar Makelov, Ludwig Schmidt, Dimitris Tsipras, and Adrian Vladu. Towards deep learning models resistant to adversarial attacks, 2019. 2, 5
- [17] Shenhan Qian, Tobias Kirschstein, Liam Schoneveld, Davide Davoli, Simon Giebenhain, and Matthias Nießner. Gaussianavatars: Photorealistic head avatars with rigged 3d gaussians. In *Proceedings of the IEEE/CVF Conference on Computer Vision and Pattern Recognition*, pages 20299–20309, 2024. 3, 4
- [18] Jérôme Rony, Luiz G Hafemann, Luiz S Oliveira, Ismail Ben Ayed, Robert Sabourin, and Eric Granger. Decoupling direction and norm for efficient gradient-based l2 adversarial attacks and defenses. In *Proceedings of the IEEE/CVF conference on computer vision and pattern recognition*, pages 4322–4330, 2019. 11
- [19] Sefik Serengil and Alper Ozpinar. A benchmark of facial recognition pipelines and co-usability performances of modules. *Journal of Information Technologies*, 17(2):95–107, 2024. 8
- [20] Shawn Shan, Emily Wenger, Jiayun Zhang, Huiying Li, Haitao Zheng, and Ben Y. Zhao. Fawkes: Protecting privacy against unauthorized deep learning models. In *29th USENIX Security Symposium (USENIX Security 20)*, pages 1589–1604. USENIX Association, 2020. 2, 3
- [21] Maitreya Suin, Kuldeep Purohit, and A. N. Rajagopalan. Spatially-attentive patch-hierarchical network for adaptive motion deblurring. In *2020 IEEE/CVF Conference on Computer Vision and Pattern Recognition (CVPR)*, pages 3603–3612, 2020. 3
- [22] Yuhao Sun, Lingyun Yu, Hongtao Xie, Jiaming Li, and Yongdong Zhang. Diffam: Diffusion-based adversarial makeup transfer for facial privacy protection. In *Proceedings of the IEEE/CVF conference on computer vision and pattern recognition*, pages 24584–24594, 2024. 3
- [23] Xinyi Tu and Bruna De Castro e Silva. Are we ready for the metaverse? implications, legal landscape, and recommendations for responsible development. *Digital Society*, 4(1):9, 2025. 2
- [24] Hang Wang, Huansheng Ning, Yujia Lin, Wenxi Wang, Sahraoui Dhelim, Fadi Farha, Jianguo Ding, and Mahmoud Daneshmand. A survey on the metaverse: The state-of-the-art, technologies, applications, and challenges. *IEEE Internet of Things Journal*, 10(16):14671–14688, 2023. 2
- [25] Yunqian Wen, Bo Liu, Li Song, Jingyi Cao, and Rong Xie. Differential private identification protection for face images. In *Face De-identification: Safeguarding Identities in the Digital Era*, pages 75–108. Springer, 2024. 8
- [26] Ethan Wilson, Vincent Bindschaedler, Sophie Jörg, Sean Sheikholeslam, Kevin Butler, and Eakta Jain. Towards privacy-preserving photorealistic self-avatars in mixed reality. *arXiv preprint arXiv:2507.22153*, 2025. 6
- [27] Haoxin Yang, Xuemiao Xu, Cheng Xu, Huaidong Zhang, Jing Qin, Yi Wang, Pheng-Ann Heng, and Shengfeng He. G<sup>2</sup>face: High-fidelity reversible face anonymization via generative and geometric priors. *IEEE Transactions on Information Forensics and Security*, 19:8773–8785, 2024. 3
- [28] Wang Yifan, Felice Serena, Shihao Wu, Cengiz Öztireli, and Olga Sorkine-Hornung. Differentiable surface splatting for point-based geometry processing. *ACM Transactions on Graphics*, 38(6), 2019. 4
- [29] Haoyu Zhai, Shuo Wang, Pirouz Naghavi, Qingying Hao, and Gang Wang. Restoring gaussian blurred face images for deanonymization attacks, 2025. 3

## Appendix A. Extended Ablation Study

### A.1. Attacks on Different Gaussian Avatar Components

Here we investigate the effect of adversarial perturbations applied to components of the 3D Gaussian Splatting avatar representation beyond the DC (base color) coefficients. Specifically, we evaluate attacks on: (1) AC coefficients (higher-order spherical harmonics), (2) Gaussian positions, (3) scale, (4) rotation, and (5) opacity.

For each component, we perform  $\ell_\infty$ -bounded PGD with 300 iterations and a privacy budget of  $\epsilon = 0.1$ , keeping evaluation protocols identical to the DC-based attack used in AEGIS. Evaluation results (for AdaFace) are summarized in Table 4, with qualitative comparisons shown in Figure 5.

The results reveal two characteristic failure modes among non-DC attacks: insufficient identity suppression and severe fidelity degradation. Perturbing opacity, rotation, or scale yields no privacy benefit (each achieves 100% Rank-1, Rank-50, and Match Rate) indicating that the AdaFace verifier consistently recovers the true identity. Conversely, perturbing AC coefficients or positions disrupts identity but introduces substantial artifacts. The AC attack attains complete identity obfuscation (0% match rate) but drastically harms reconstruction quality (SSIM 0.6515; PSNR 22.61) and semantic attribute preservation (age difference 8.84; emotion match accuracy 40%). Position perturbation offers partial identity suppression (20% Rank-50 and Match Rate) yet still reduces fidelity (SSIM 0.8935), falling short of AEGIS.

Restricting perturbations to DC coefficients allows AEGIS to preserve the underlying Gaussian geometry and thus maintain high perceptual and semantic fidelity. Among all evaluated strategies, AEGIS uniquely satisfies both objectives, achieving complete de-identification, while preserving high perceptual consistency.

Method	Rank 1 (%) ↓	Rank 50 (%) ↓	Match rate (%) ↓	SSIM ↑	PSNR (dB) ↑	Age (diff.) ↓	Race (%) ↑	Gender (%) ↑	Emotion (%) ↑
<b>AEGIS</b>	<b>0</b>	<b>0</b>	<b>0</b>	<b>0.9555</b>	<b>35.52</b>	<b>2.62</b>	<b>60</b>	<b>100</b>	<b>80</b>
AC	0	0	0	0.6515	22.61	8.84	50	90	40
opacity	100	100	100	0.9977	51.69	0.49	90	100	90
position	0	20	20	0.8935	30.29	2.88	80	90	90
rotation	100	100	100	0.9795	37.39	0.92	90	100	100
scale	100	100	100	0.9927	43.78	1.01	90	100	90

Table 4. Quantitative evaluation of adversarial attacks applied to different components of the 3D Gaussian avatar representation, evaluated against the AdaFace verification system and compared to the best-performing AEGIS configuration.



Figure 5. Qualitative comparison of adversarial perturbations applied to different components of the 3D Gaussian avatar representation. Each row shows the resulting masked avatar under attacks targeting AC coefficients, opacity, position, rotation, and scale, contrasted with the best-performing AEGIS configuration.

By limiting perturbations to only the DC components, AEGIS ensures the the avatar’s geometry remains unaltered, therefore preserving perceptual realism and utility of the avatar. AEGIS is the only method to successfully achieve the required dual objective. It alone provides perfect identity protection (0% match rates) while maintaining the highest visual fidelity (0.9555 SSIM, 35.52 PSNR) and the best overall semantic attribute preservation among all effective methods.

### A.2. Different Adversarial Optimization Strategies

We extend our ablation by evaluating a broader set of adversarial optimization strategies, including both  $\ell_\infty$  and Euclidean ( $\ell_2$ ) perturbation regimes. Beyond the iterative PGD attack used in AEGIS, we consider two additional families of methods. First, we apply the Fast Gradient Sign Method (FGSM) [8], a single-step linearization that perturbs parameters in the direction of the gradient sign. Second, we adopt the Decoupled Direction and Norm (DDN) attack [18], which iteratively optimizes

perturbations by separating the gradient direction from the update magnitude, thereby seeking the minimal  $\ell_2$  norm necessary to induce a successful attack.

In the high-dimensional DC coefficient space, directly converting our  $\ell_\infty$  budget ( $\epsilon_\infty = 0.1$ ) into its  $\ell_2$  equivalent yields  $\epsilon_2 = \epsilon_\infty \sqrt{d}$ , where  $d$  denotes the dimensionality of the DC tensor. Empirically, this scaling produces large perturbation magnitudes that introduce severe and visually unacceptable distortions. To obtain a more realistic perturbation scale, we rely on DDN to estimate the minimal effective  $\ell_2$  norm required for adversarial success. DDN converges to an average perturbation magnitude of approximately  $\|\cdot\|_2 \approx 5$ . Motivated by this finding, and by the observation that smaller fixed budgets fail to suppress identity, we set the  $\ell_2$  radius for fixed-budget attacks to  $\epsilon_2 = 10$ . Quantitative comparisons for all  $\ell_\infty$  and  $\ell_2$  adversarial strategies are presented in Table 5, with qualitative visualizations provided in Figure 6.

Method	Rank	Rank	Match rate	SSIM $\uparrow$	PSNR	Age	Race	Gender	Emotion
	1 (%) $\downarrow$	50 (%) $\downarrow$	(%) $\downarrow$		(dB) $\uparrow$	(diff.) $\downarrow$	(%) $\uparrow$	(%) $\uparrow$	(%) $\uparrow$
<b>AEGIS</b>	<b>0</b>	<b>0</b>	<b>0</b>	<b>0.9555</b>	<b>35.52</b>	<b>2.62</b>	<b>60</b>	<b>100</b>	<b>80</b>
DDN	80	90	90	0.9861	41.67	2.21	90	90	100
$\ell_2$ -PGD ( $\epsilon = 5$ )	10	60	60	0.9785	39.32	2.64	80	90	90
$\ell_2$ -PGD ( $\epsilon = 10$ )	0	0	0	0.9490	34.40	4.23	50	90	100
$\ell_\infty$ -FGSM ( $\epsilon = 0.1$ )	100	100	100	0.9516	35.84	3.55	70	90	80
$\ell_2$ -FGSM ( $\epsilon = 5$ )	100	100	100	0.9778	39.02	2.36	60	90	80
$\ell_2$ -FGSM ( $\epsilon = 10$ )	90	100	100	0.9390	33.23	4.97	50	90	70

Table 5. Quantitative comparison of different adversarial optimization strategies under  $\ell_\infty$  and  $\ell_2$  constraints, evaluated against the AdaFace verification system and compared to the best-performing AEGIS configuration.

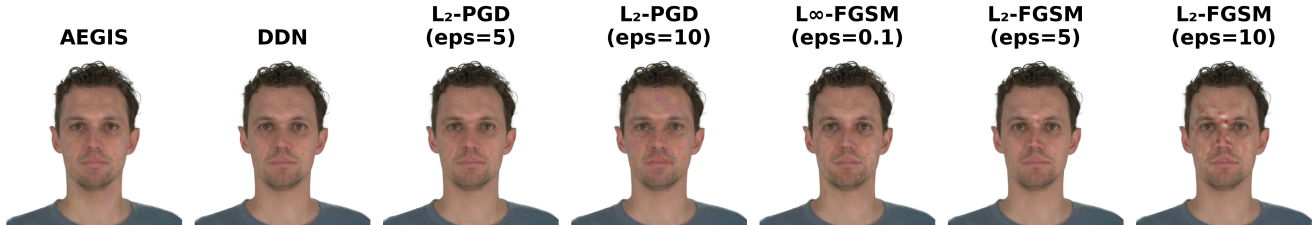


Figure 6. Qualitative comparison of identity masking results produced by different adversarial optimization strategies (DDN, PGD, FGSM under  $\ell_\infty$  and  $\ell_2$  norms), shown alongside the best-performing AEGIS configuration.

Across all evaluated optimization methods, AEGIS is the only approach that simultaneously achieves complete identity suppression and high perceptual fidelity. Among  $\ell_2$ -based attacks, both DDN and low-budget  $\ell_2$ -PGD ( $\epsilon = 5$ ) fail to reliably break verification, producing match rates of 90% and 60%, respectively. Increasing the perturbation radius to  $\epsilon = 10$  enables  $\ell_2$ -PGD to reduce the match rate to 0%, but this comes at the expense of fidelity degradation (SSIM drops to 0.9490 and the age difference increases to 4.23). Single-step FGSM variants perform worst overall, with both  $\ell_\infty$  and  $\ell_2$  FGSM achieving match rates close to 100%, indicating that they are unable to generate sufficiently targeted yet visually subtle perturbations. Overall, these results show that naive or low-budget  $\ell_2$  attacks are ineffective for identity obfuscation, while larger  $\ell_2$  budgets compromise fidelity.

## Appendix B. Additional Examples

### B.1. Masking Persistence Under Rotation

We further evaluate the robustness of our identity masking to changes in viewpoint. Figure 7 illustrates renderings of the unprotected avatar across a grid of camera poses, covering pitch and yaw values linearly sampled in the range  $[-0.8, 0.8]$  radians. As shown, the subject’s identity remains clearly recognizable across nearly all viewpoints.

Figure 9 presents the same avatar after applying AEGIS with  $\epsilon = 0.1$ , rendered from the identical set of camera positions. The perturbation remains stable under rotation, yielding consistent suppression of identifiable facial characteristics across the complete viewing grid.

These observations are corroborated by the similarity-score distributions in Figures 8 and 10. The unprotected avatar exhibits a distribution concentrated above the verification threshold, indicating reliable identity recognition under pose vari-

ation. In contrast, the protected avatar produces a distribution shifted decisively below the threshold, demonstrating that AEGIS maintains effective identity masking over a wide range of viewing angles.

## **B.2. Additional Samples Visualization**

We include in Figure 11 an expanded set of avatar renderings for all methods evaluated in Table 2. These qualitative examples illustrate the characteristic visual behavior of each approach across a diverse set of subjects, complementing the quantitative results.

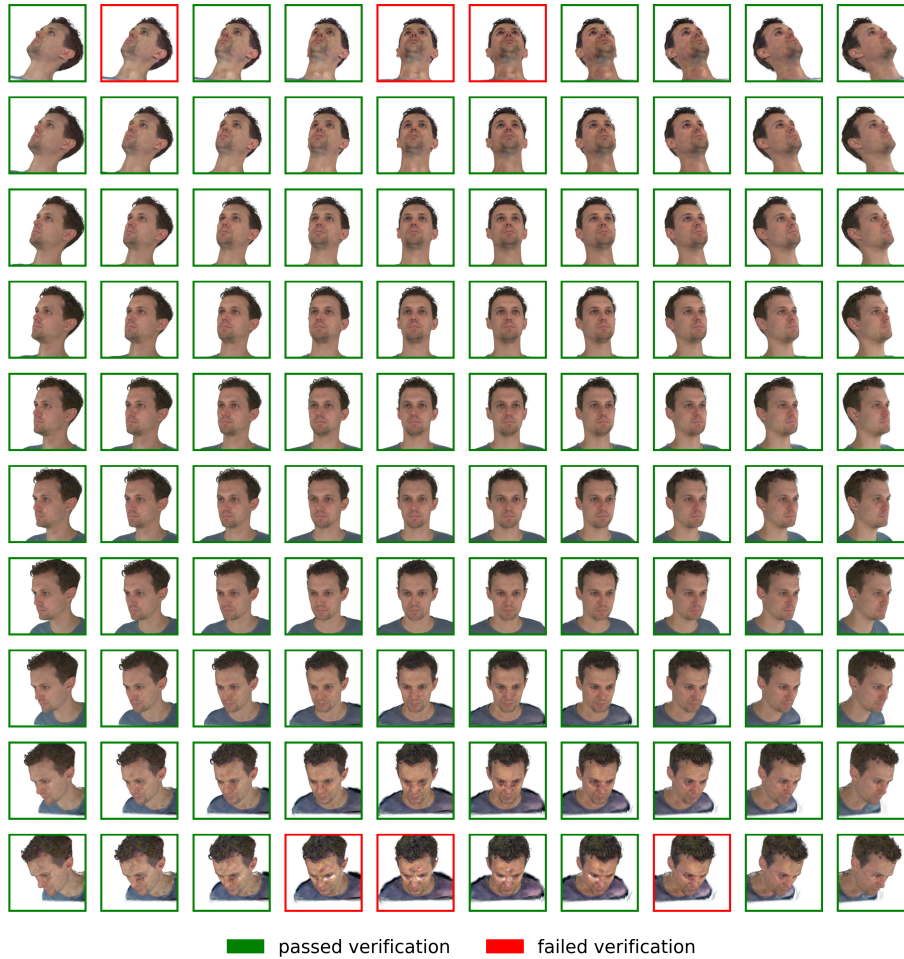


Figure 7. Verification results obtained by the AdaFace system across various rotation angles (poses) for the original, unmasked avatar.

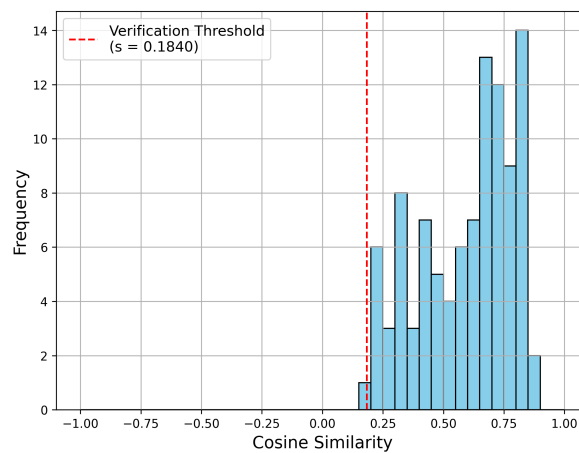


Figure 8. Histogram showing the distribution of cosine similarities between the original avatar's rotated renders and the NeRSebmlcGT reference photos. The renders correspond to the poses presented in Figure 7.

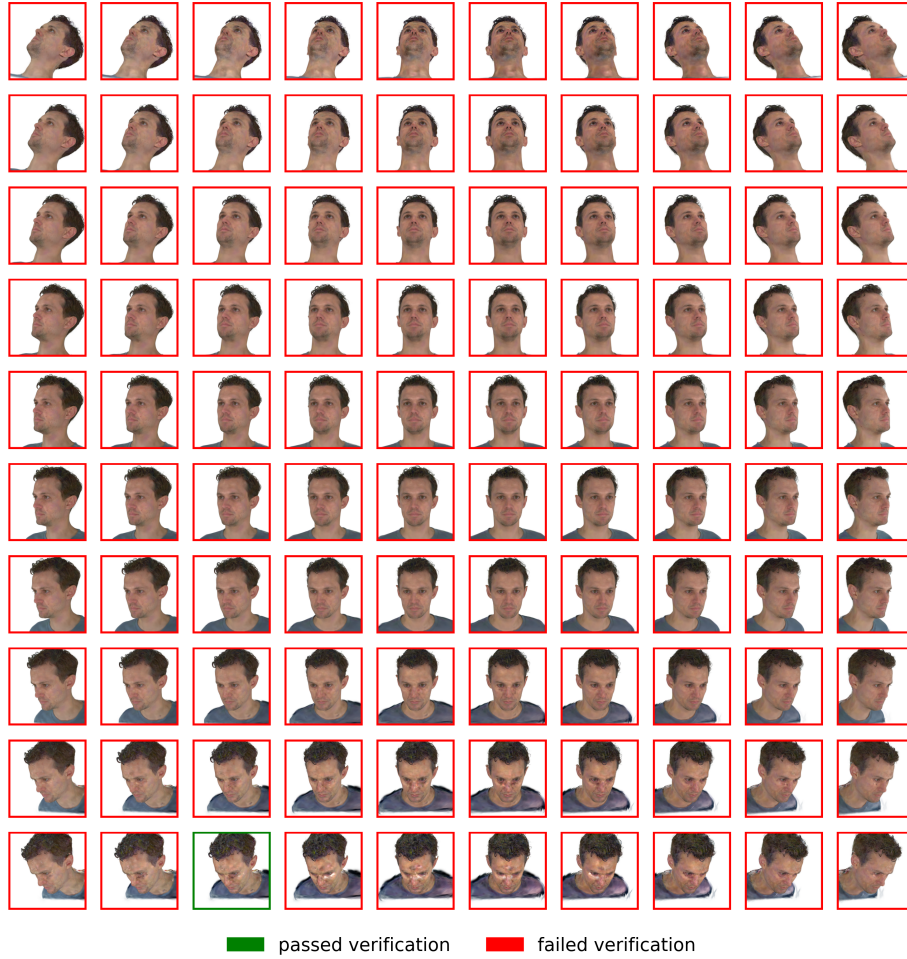


Figure 9. Verification results obtained by the AdaFace system for the avatar protected using the AEGIS method with  $\epsilon = 0.1$ , shown across various rotation angles.

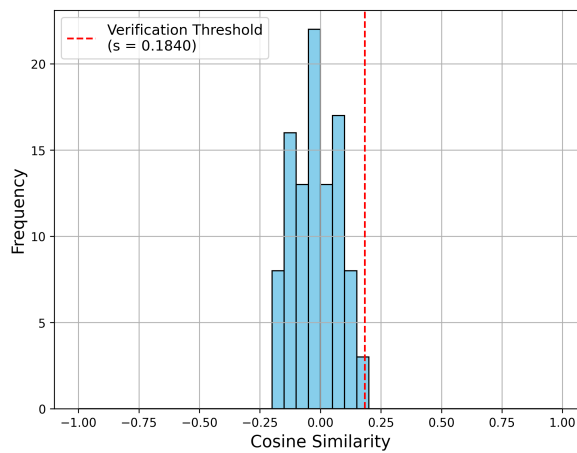


Figure 10. Histogram showing the distribution of cosine similarities between the AEGIS masked avatar's rotated renders and the NeRSebm-leGT reference photos. The renders correspond to the poses presented in Figure 9.



Figure 11. Extended qualitative visualization of avatar masking results for all configurations evaluated in Table 2. (Top)



(Bottom) Continuation of Fig. 11.